Thin–Walled Structures 160 (2021) 107345

Contents lists available at ScienceDirect

Thin-Walled Structures

journal homepage: http://www.elsevier.com/locate/tws

Semi-rigid floor-to-wall connections using side-framed lightweight steel structures: Concept development

Alireza Bagheri Sabbagh [a,*], Shahabeddin Torabian [b,c]

[a] School of Engineering, University of Aberdeen, Scotland, UK
[b] Simpson Gumpertz & Heger, Inc., Washington DC, USA
[c] Department of Civil and Systems Engineering, Johns Hopkins University, Baltimore, MD, USA

ARTICLE INFO

Keywords:
Lightweight steel framing
Semi-rigid connections
Connection rotational stiffness

ABSTRACT

This paper presents the development of side-framed lightweight steel (SFLS) structures featuring semi-rigid floor-to-wall connections. Initially, the effect of variation of connection rotational stiffness on the design of a two-storey frame is investigated considering different construction methods. The results revealed a considerable effect of the connection rotational stiffness on the design of the joists and studs. A semi-rigid connection is then developed using validated finite element analyses. The developed SFLS system enables more efficient designs addressing the predominant limit states of the conventional designs with fewer and lighter flooring members and connections.

1. Introduction

Typical best-practice lightweight steel framing (LSF) systems comprising cold-formed steel (CFS) stud walls and joisted floors include platform framing, ledger framing, and balloon framing [1]. These systems are being constructed using two different methods: (i) a sequential construction method (SCM) for platform and ledger framing, with floors and walls of one storey level built at a time with no stud continuity between the upper and lower storey walls, and (ii) a continuous construction method (CCM) for balloon framing, with the wall studs being spliced above the floor levels providing continuity between the adjacent storeys [1]. The flooring joists are either supported on top of the wall studs capped with a top track (in platform framing) or attached to the face of the walls (in both ledger and balloon framing). The floor-to-wall connections are generally categorised as simply supported designed to transfer shear or bearing forces to the wall frame [1,2]. The design of the joisted floors is generally dominated by the mid-span deflection serviceability limit state leading to relatively heavy flooring joists [1–3].

In recently completed experiments on ledger-framed LSF floor-to-wall connections [3] comprising floor joists connected to the face of the wall studs, various types of premature local failure limit states have been identified in the components of the floor-to-wall connections. These include ledger flange buckling, stud web crippling, and fastener pull-out, which were identified as the dominant ultimate limit states [2]. These occur primarily due to the imposed eccentricity and the consequential out-of-plane actions within the floor-to-wall connection associated with the positioning of a single flooring joist relative to the location of adjacent wall studs. The identified limit states, which are not included in the current design practice, can compromise the gravity load-bearing system under extreme loading conditions [3]. To mitigate these failure limit states, a recommendation is to increase the stud thickness matching or greater than the joist thickness [3]. This approach, however, can lead to an overly conservative design with a significant portion of underutilised strength of the stud sections.

A side-framed lightweight steel (SFLS) system comprising semi-rigid floor-to-wall connections is developed herein for a more efficient joist-stud framed design. The proposed system postpones or even eliminates local failure limit states within the connection components due to the zero eccentricity in the connection which has been identified as the primary source of the local failures in the ledger-framed connections. These local failures, as discussed above, could affect the design of the wall studs towards higher thickness sections [2]. The semi-rigid connections reduce the mid-span deflection of the joisted floors which has been recognised [3] as the governing limit state for the typical CFS floor systems. Furthermore, the SFLS system requires fewer number of members and connections, compared with the ledger-framed systems, eliminating a ledger beam per side of a wall and a clip angle connection per joist.

* Corresponding author.
E-mail addresses: alireza.bsabbagh@abdn.ac.uk (A. Bagheri Sabbagh), storabian@sgh.com (S. Torabian).

https://doi.org/10.1016/j.tws.2020.107345
Received 15 September 2020; Received in revised form 28 November 2020; Accepted 29 November 2020
Available online 11 December 2020
0263-8231/

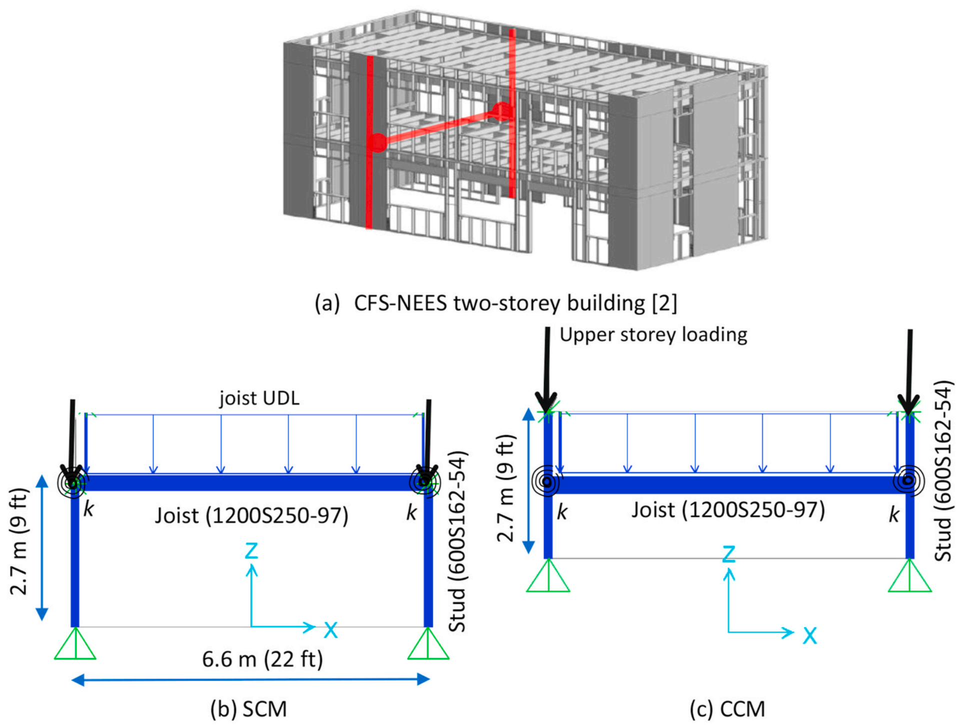

Fig. 1. Lower storey joist-stud framed SCM and CCM configurations adopted from CFS-NEES two-storey building [2].

Initially, a general trend for the effect of incorporation of semi-rigid connections on the design of an archetype building, two-storey CFS-NEES building [2], is studied. The SFLS system is developed and assessed using finite element (FE) models featuring both the SCM and CCM designs. A stiffness estimation model is then developed for the semi-rigid SFLS connection and compared against the FE results.

2. Two-storey CFS-NEES building frame assessment with semi-rigid connections

2.1. Joist-stud framed model specifications

A two-storey single-span joist-stud framed model is adopted from the CFS-NEES building design (schematically shown in Fig. 1 (a)) [2]. The focus herein is on the design of the lower storey level joist and stud sections varying the joist-to-stud connection rotational stiffness (k). Both the sequential and continuous construction methods (SCM and CCM) have been considered, with their frame models, respectively shown in Fig. 1 (b) and (c). Half-height studs were modelled for the CCM configuration representing the inflection points of the studs. For the SCM configuration, a restraining point is assumed at the half-height of the studs accounting for the bridging. Through-fastened to floor sheathing condition is assumed for the design of the joists as laterally braced members. Both of these boundary conditions for the joists and studs were defined as the design criteria within the computational model. The span length of 6.6 m and height of 2.7 m are taken from the CFS-NEES design narrative [2]. The flooring joists are laid down 600 mm on-centre, which are subjected to a uniform distributed loading (UDL) of 3.5 kN/m^2 (LL: Live Load) and 1.0 kN/m^2 (DL: Dead Load), adopted from the design narrative [2]. The upper storey roof loading is transferred to the lower storey studs through the point loads of 2.0 kN (LL) and 3.0 kN (DL) as per [2].

The 1200S250-97 joist and 600S162-54 stud lipped sections (with the web depths of 304 and 152 mm, flange widths of 64 and 41 mm and thicknesses of 2.5 and 1.4 mm, respectively), using the AISI S240 [4] nomenclature, have been adopted from the CFS-NEES narrative [2], which were designed based on the nominal yielding strength of 345 MPa and modulus of elasticity of 203,500 MPa. These are considered herein as the benchmark designs for both the SCM and CCM joist-stud frames. An imposed eccentricity of $e = 76$ mm between the face of the stud wall to the centre line of the stud section was considered in the design process [2] to transfer the joist shear force to the wall studs.

Table 1
SCM joist-stud framed design.

k (kN.m/rad)	Joist section[a]	Joist DCR		Stud section[a]	Stud DCR
0 ($e = 76$ mm)	1200S250-97	0.76 (M)	0.92 (D)	600S162-54	0.73 ($M + C$)
103 ($e = 76$ mm)	1200S250-97	0.73 (M)	0.87 (D)	600S162-54	0.89 ($M + C$)
500 ($e = 0$)	1200S250-97	0.72 (M)	0.85 (D)	600S162-54	1.01 ($M + C$)
1000 ($e = 0$)	1200S250-97	0.69 (M)	0.80 (D)	600S162-68	0.91 ($M + C$)
2000 ($e = 0$)	1200S250-97	0.68 (M)	0.78 (D)	600S162-68	0.97 ($M + C$)
3000 ($e = 0$)	1200S250-68	1.06 (M)	0.94 (D)	600S162-97	0.91 ($M + C$)
5000 ($e = 0$)	1200S250-68	1.05 (M)	0.93 (D)	600S162-97	0.93 ($M + C$)
10000 ($e = 0$)	1200S250-68	1.04 (M)	0.92 (D)	600S162-97	0.95 ($M + C$)
Fully-Fixed ($e = 0$)	1200S250-68	1.03 (M)	0.90 (D)	600S162-97	0.98 ($M + C$)

[a] 1200S250- joist and 600S162- stud lipped sections with the web depths of 304 and 152 mm and flange widths of 64 and 41 mm; the two-digit number after dash refers to the section thicknesses of 1.4 mm (54), 1.8 mm (68) and 2.5 mm (97).

2.2. Joist-stud framed model results and discussions

The joist-stud framed models have been analysed employing CSI SAP2000 [5] and designed based on AISI-S100-2016. Tables 1 and 2 list the designed joist and stud sections and their corresponding Demand-to-Capacity Ratios (DCRs) for SCM and CSM frames, respectively. These are related to a wide range of the connection rotational stiffness (k) from a simply supported frame (the benchmark design) to a fully fixed frame. The joist design limit states include mid-span bending moment, denoted by M; the bending moment and shear force combined effect at the joist end location, denoted by $M + V$; and the mid-span deflection, limited to lesser of span length/240 for DL + LL or length/360 for LL [2], denoted by D. The stud is designed based on the combined bending moment and compression force, denoted by $M + C$.

Table 2
CCM joist-stud framed design.

k (kN.m/rad)	Joist section[a]	Joist DCR		Stud section[a]	Stud DCR
0 (e = 76 mm)	1200S250-97	0.75 (M)	0.92 (D)	600S162-54	0.62 ($M + C$)
103 (e = 76 mm)	1200S250-97	0.71 (M)	0.85 (D)	600S162-54	0.74 ($M + C$)
500 (e = 0)	1200S250-97	0.65 (M)	0.76 (D)	600S162-54	0.92 ($M + C$)
1000 (e = 0)	1200S250-68	0.94 (M)	0.85 (D)	600S162-68	0.92 ($M + C$)
2000 (e = 0)	1200S250-68	0.87 ($M + V$)	0.76 (D)	600S162-68	1.02 ($M + C$)
3000 (e = 0)	1200S250-68	0.96 ($M + V$)	0.66 (D)	600S162-97	0.77 ($M + C$)
5000 (e = 0)	1200S250-68	1.00 ($M + V$)	0.62 (D)	600S162-97	0.80 ($M + C$)
10000 (e = 0)	1200S250-68	1.03 ($M + V$)	0.59 (D)	600S162-97	0.82 ($M + C$)
Fully-Fixed (e = 0)	1200S250-68	1.08 ($M + V$)	0.55 (D)	600S162-97	0.85 ($M + C$)

[a] 1200S250- joist and 600S162- stud lipped sections with the web depths of 304 and 152 mm and flange widths of 64 and 41 mm; the two-digit number after dash refers to the section thicknesses of 1.4 mm (54), 1.8 mm (68) and 2.5 mm (97).

To minimise the variation of the joist and stud cross-sections, the overall dimension of the joist and stud sections were kept the same as those of the benchmark designs. In total three sets of joist and stud cross-sections have been designed corresponding to the three identified ranges of the connection rotational stiffnesses of $k \leq 500$, $500 < k \leq 2000$ and $k > 2000$ kN m/rad (see Tables 1 and 2 for SCM and CCM, respectively). For better comparison, Fig. 2 illustrates the average trend of the DCRs for both the SCM and CCM designs.

For the benchmark design with $k = 0$, the joist deflection dominates the design with DCR ratio of 0.92 (for both SCM and CCM designs) complying with the CFS-NEES design narrative [2]. The connection rotational stiffness of $k = 103$ kN m/rad is adopted from the recently completed experiments for the ledger-framed floor-to-wall connections (test T5 reported in Ref. [3]). Compared with the benchmark design, the stud DCR is increased by 22% from 0.73 to 0.89 and dominate the SCM design, while the deflection DCR is reduced 5% from 0.92 to 0.87. For the CSM design, the stud DCR is also increased by 19% from 0.63 to 0.75. This indicates that even a low level of connection rotational stiffness, which is generally being ignored in the joist-stud framed design [2], can noticeably affect the overall design towards an unconservative side. The unconservative design might arise when the initial DCR is close to unity, and the additional demands due to partial fixity would push the stud DCR above unity, thus requiring a larger stud section. This effect can result in unexpected failures in wall studs under extreme loading conditions (i.e. wind or seismic), even compromising the gravity loading system.

For joist-stud framed designs with higher connection rotational stiffness ($k = 500$ kN m/rad and beyond), the connection eccentricity of $e = 0$ is assumed consistent with the details of the SFLS semi-rigid connections discussed in the following sections. Variation of the connection rotational stiffness from simply supported (benchmark design) to fully fixed conditions has resulted in the joist and stud sections, with the same overall dimensions, ranging three sets of thicknesses of 97-54, 97-68, and 68–97 mils for SCM design, and 97-54, 68-68, and 68–97 mils for CSM design. The section thicknesses of 54, 68 and 97 in mils unit are respectively equivalent to 1.4, 1.8 and 2.5 mm in SI units. The overall trend is shifting from a heavier joist section (having 97 mils thickness) governed by deflection (deemed undesirable) for the lower k values towards a 28% lighter joist section (having 68 mils thickness) governed by strength (deemed desirable) for the higher k values. This is more noticeable for the CCM design and has been achieved at $k = 1000$ kN m/rad, while $k = 3000$ kN m/rad is the minimum stiffness level for the joists to be dominated by strength in the SCM design. This is attributed to the higher CCM joist-stud framed stiffness compared with that of the SCM design. Heavier stud sections (having 68 or 97 mils thicknesses) are, however, required for both the SCM and

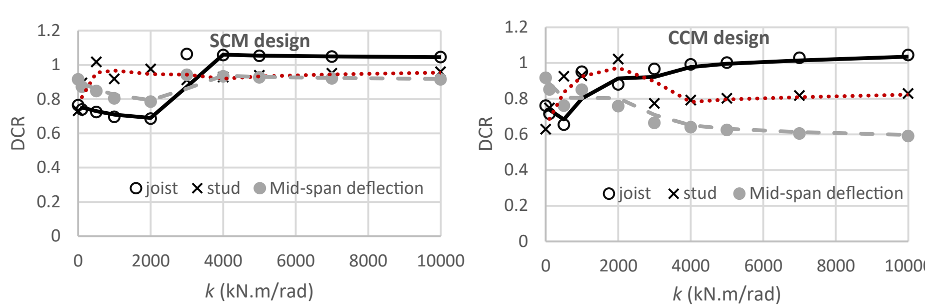

Fig. 2. Average trends for joist and stud DCRs for SCM and CCM designs.

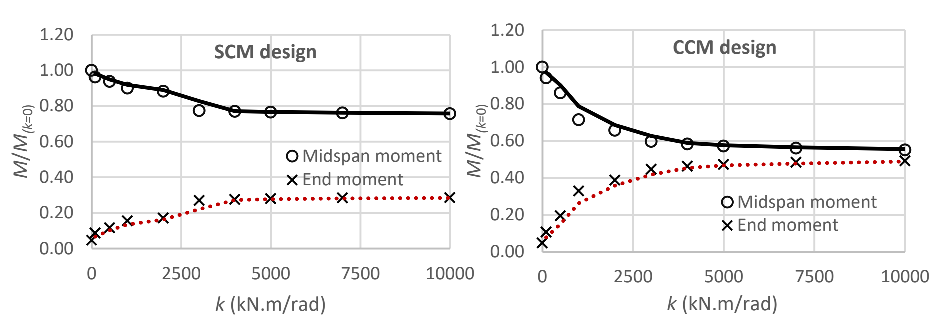

Fig. 3. Averaged trend for joist mid-span and end bending moments for SCM and CCM designs.

C9754-1,2,3 or 4

Table 3
SFLS FE models.

Label[a]	Construction	Joist section	Stud section	Vertical screw lines
S9754-1,2,3 or 4	SCM	1200S250-97	600S162-54	
	CCM	1200S250-97	600S162-54	
S6868-1,2,3 or 4	SCM	1200S250-68	600S162-68	
C6868-1,2,3 or 4	CCM	1200S250-68	600S162-68	
S9768-1,2,3 or 4	SCM	1200S250-97	600S162-68	
C9768-1,2,3 or 4	CCM	1200S250-97	600S162-68	
S6897-1,2,3 or 4	SCM	1200S250-68	600S162-97	
C6897-1,2,3 or 4	CCM	1200S250-68	600S162-97	

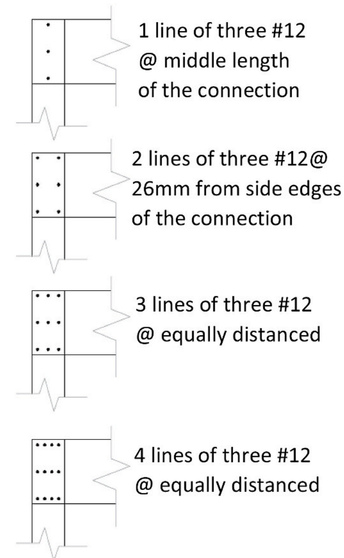

[a] Definition of the labels: letters S and C stand for SCM and CCM; 4-digit number (9754, 6868, 6897 and 9768) represent the thickness of joist and stud sections: 1.4 mm (54), 1.8 mm (68) and 2.5 mm (97); single-digit number after dash refers to the vertical lines of #12 screws.

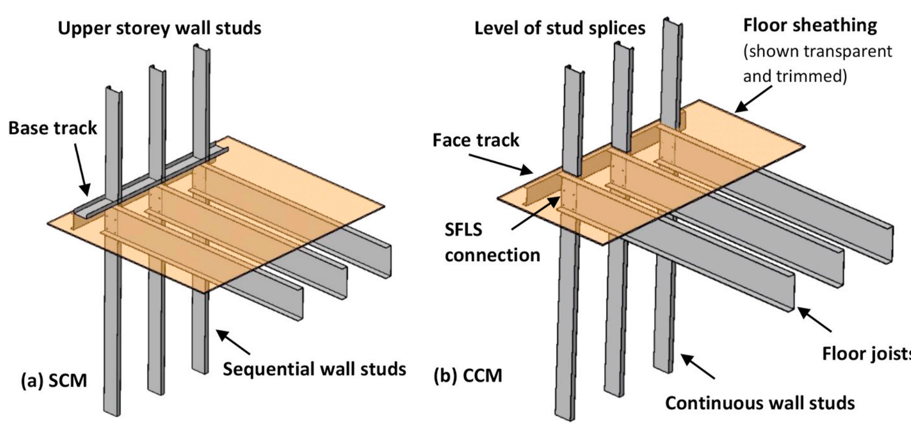

Fig. 4. Schematic drawing of the SFLS floor-to-wall connection system for both (a) SCM and (b) CCM.

CCM designs due to the larger bending moments imposed to the studs at higher k values.

In general, the CCM design can provide a more uniform joist bending moment distribution, that can be observed in Fig. 3. The figure shows a smaller gap between the averaged trends of the mid-span and end moments (normalised by the mid-span M for the benchmark design with $k = 0$) for the CCM design compared with that of the SCM design. The more economical design could be achieved for k values in the range of $500 < k \leq 2000$ kN m/rad with a lighter joist section having 68 mils thickness for CCM compared with 97 mils for SCM designs. However, the higher CCM joist end bending moment values (shown in Fig. 3) caused the combined moment and shear effect ($M + V$) to govern in the design with $k = 2000$ kN m/rad and beyond (with the high DCRs of 0.87 and above, referring to Table 3). This resulted in the same joist section of 1200S250-68 for both SCM and CCM designs with $k = 3000$ kN m/rad and beyond, governed by M and $M + V$, respectively.

3. Side-framed lightweight steel system with semi-rigid connections

Within this section, a side-framed lightweight steel (SFLS) flooring joist-to walling stud semi-rigid connection has been detailed and assessed under distributed gravity loading. In this system, the flooring joists are attached to the side of the walling studs through a planar screw connection pattern, schematically shown in Fig. 4 (a) and (b) for SCM and CCM, respectively. The imposed eccentricity within the recently tested ledger-framed connections [3], which causes unavoidable out-of-plane actions and local failures (which may end up in a larger stud thickness), would, therefore, be eliminated within the SFLS type of connection. Furthermore, compared with the ledger-framed systems, the ledger beams and the joist-to-ledger clip angle connections are eliminated, which together with the lighter joist sections using semi-rigid connections (see Section 2) can potentially lead to a more efficient and economical LSF system.

When the joists are not continuous (for the case of alternate joist orientation or external walls), a face-track (shown in Fig. 4 (a) and (b)) could run at the opposite side of the wall and is attached to the wall studs

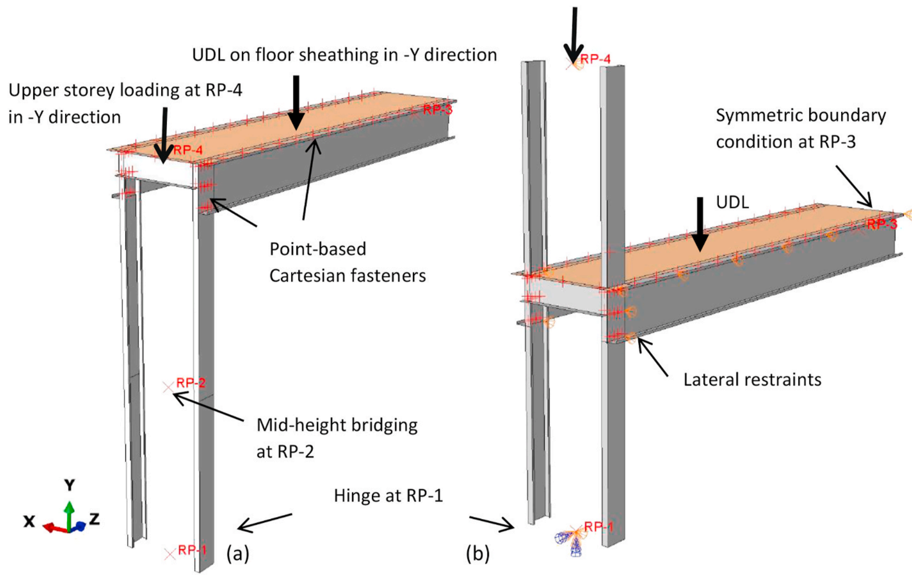

Fig. 5. Overall view for (a) SCM and (b) CCM FE models: Boundary conditions, loading and fasteners.

(in lieu of the conventional top tracks). The face-track provides a lateral restraining effect for the studs and supports the floor and wall sheathings. The in-plane strap braces, if present, can be connected to the face of the studs below or above the joist levels with no interference with the face tracks which are levelled with the joist top flanges and are typically shallower than the joists. When the joists are extended to the opposite side of the walls, the face tracks can be placed in segments between the studs. Fig. 4(a) and (b) also shows a wood-based sheathing attached to the top of the joists which can be extended to the opposite side of the walls for the case of alternate joist orientation.

A detailed finite element analysis using ABAQUS [6] has been employed to model the SFLS flooring joist-to-walling stud semi-rigid connections. The main features of the finite element (FE) models have been firstly validated against a tested configuration of the ledger-framed floor-to-wall connections [3]. The validated FE models are then used to assess the SFLS connections based on a range of joist and stud sections taken from the results of the SCM and CCM joist-stud framed designs presented in the previous section.

3.1. SFLS FE modelling specifications

Fig. 5 (a) and 5 (b) show typical SFLS FE models for both the SCM and CCM configurations, respectively, comprising a double joisted sheathed floor connected to the wall studs. The overall joist and stud dimensions and the floor UDL and the upper storey loading are the same as those of the design given in Section 1 (adopted from the CFS-NEES project [2]). A hinge boundary condition is applied at the base section of the studs to the reference point RP-1, shown in Fig. 5(a) and (b), to which all the degrees of freedom of that section are coupled. Mid-height bridging restraint is applied at RP-2 in the SCM configuration coupled to the stud sections at that level. The symmetric boundary condition is applied to the mid-span section of the joists at RP-3. The upper storey loading is applied through RP-4 coupled to the studs at the top section with free translation and rotation, respectively in vertical (Y-direction) and about X-direction. The lateral supports, representing blocking restraints, are applied to the joists at the mid-span and the connection end sections.

A bi-linear stress-strain curve has been utilised for the steel with the nominal yielding strength and modulus of elasticity same as those used in the frame model (see Section 2, based on CFS-NEES narrative [2]) and the strain hardening second modulus ratio of $E/E_s = 0.01$. The joists are connected to the side face of the studs using self-drilling #12 screw

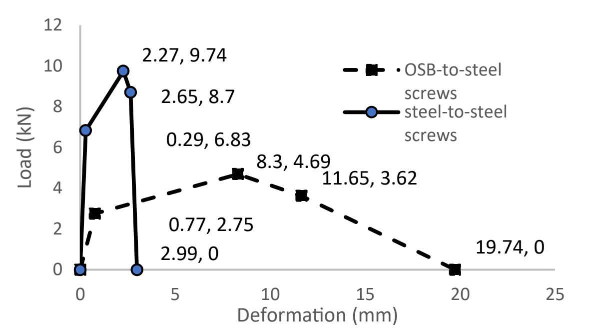

Fig. 6. Load-deformation backbone curve for steel-to-steel and OSB-to-steel #12 self-drilling screws [7].

connections with 5.4 mm thread diameter. An OSB sheathing, with a modulus of elasticity of 699 MPa [7], is attached to the top of the joists and the face track with the same #12 screws. The screw connections are modelled using Point-based Cartesian Fasteners, available in the Abaqus library, with the radius of influence equals to the thread diameter. This modelling technique has successfully been used previously in FE modelling of CFS connections [8]. Quad-linear load-deformation backbone curves, shown in Fig. 6, have been adopted from Ref. [7] for the steel-to-steel and the OSB-to-steel screw fasteners.

Nonlinear analysis has been performed using the arc-length algorithm, which takes the load magnitude as unknown and solves simultaneously for loads and displacements [6]. This method has been successfully employed in previous studies [8–10] to capture local buckling instability and incorporation of material and geometrical nonlinearity of structures. The second order S8R shell element was employed for all the steel sections having 8 nodes, each with 6 translational and rotational degrees of freedom and reduced integration. A mesh size of 10 mm × 10 mm was chosen, which shown [8,9] to capture the load-deformation response of CFS connections with high accuracy. For OSB sheathing, S4R shell type with a coarser mesh size of 50 mm × 50 mm have been adopted since the failure behaviour of OSB is not the intention of this research. Hard contact with Penalty formulation [6] has been applied between the OSB and the top surfaces of the joists and the face track. The same contact type has also been applied within the

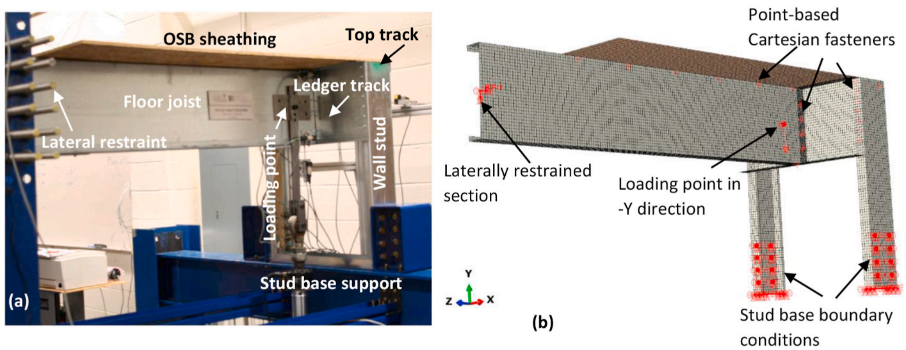

Fig. 7. (a) Leger-framed connection tests [3] and (b) FE model for specimen T4.

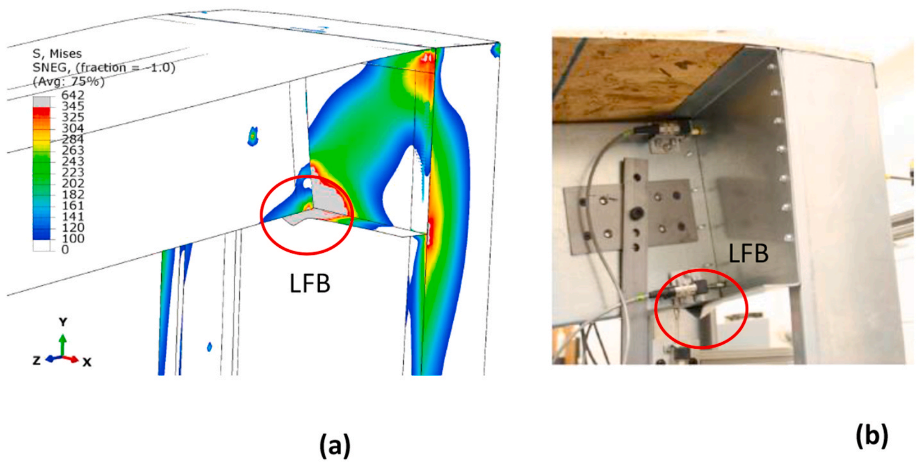

Fig. 8. (a) FE prediction and (b) T4 test ledger flange buckling for ledger-framed connection.

connection region between the surfaces of the joists, studs and the face track.

3.2. FE validation

Fig. 7 (a) shows the set up for the tests on ledger-framed connections conducted at Johns Hopkins University reported in Ref. [3]. The test specimens consist of a single 1575 mm length joist connected to a ledger track through a 38 × 38 × 1.4 mm clip angle between two 813 mm height supporting studs. The studs were supported on a test rig placed at 600 mm apart and capped with a top track. The joist, stud, ledger and top track sections were 1200S250-97, 600S162-54, 1200T200-97 and 600T162-54 respectively, all using a nominal 345 MPa yield stress, while an OSB sheathing attached to the joist flange and the top track web. All the connections employed Simpson self-drilling #10 screws with 4.7 mm thread diameter. The joint web was connected to the ledger web using four screws at each leg of the clip angle. The top and bottom flanges of the joist were connected to the ledger flanges by a single screw, while the ledger itself was connected to the stud flanges by seven screws.

Fig. 7(b) shows the FE model for the control test specimen (namely T4 in Ref. [3]) with the joist positioned at the middle length between the studs and the loading applied at 127 mm from the face of the ledger. All the modelling specifications, including the element type and sizes, contact behaviour, connection fasteners and analysis algorithm were the same as the SFLS model above. Similarly, the load-deformation behaviour of #10 screws for all the connection fasteners was adopted from the extensive single-lap tests reported in Ref. [7] using linear interpolation for the unavailable 97-54 and 54-54 steel plies. Also, the fastener pull-out load-deformation behaviour was taken from the test results

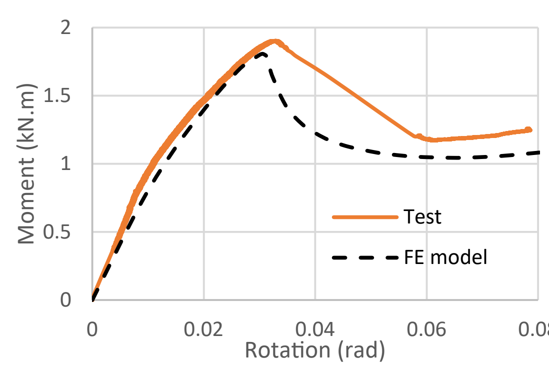

Fig. 9. Moment-rotation behaviour of the FE and T4 test ledger-framed connection.

recently published in Ref. [11]. It should be noted that the fastener pull-out failure is a critical limit state for the ledger-framed connections due to the out-of-plane nature of load transferring mechanism between the joists, ledger and studs. In SFLS connections, however, the shear behaviour is expected to be the dominant limit state (which is discussed later herein) within the proposed planar type of connection.

Fig. 8 (a) shows the ledger flange buckling (LFB) captured by the FE model which occurred in the T4 test, as can be observed in Fig. 8 (b), as the dominant failure limit state. Further, the overall trend of the moment-rotation behaviour estimated by FE analysis, as shown in Fig. 9, matches reasonably well with that of the test. The peak strength and initial stiffness predictions by the FE analysis are within 5% and 10% of those of the test, respectively. These relatively small differences could be

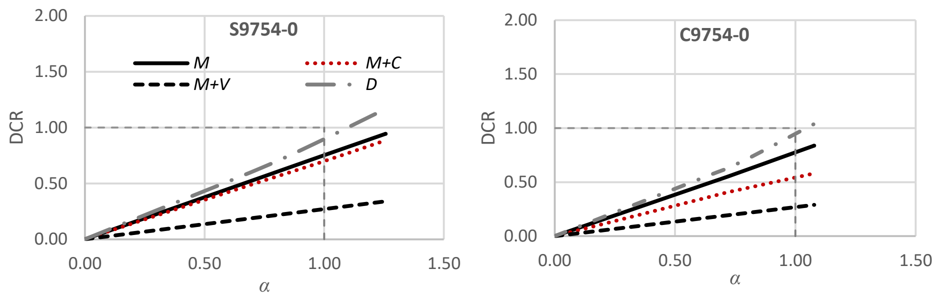

Fig. 10. Variation of DCRs with α for M, $M+V$, $M+C$, and D limit states for S9754–0 and C9754-0 designs.

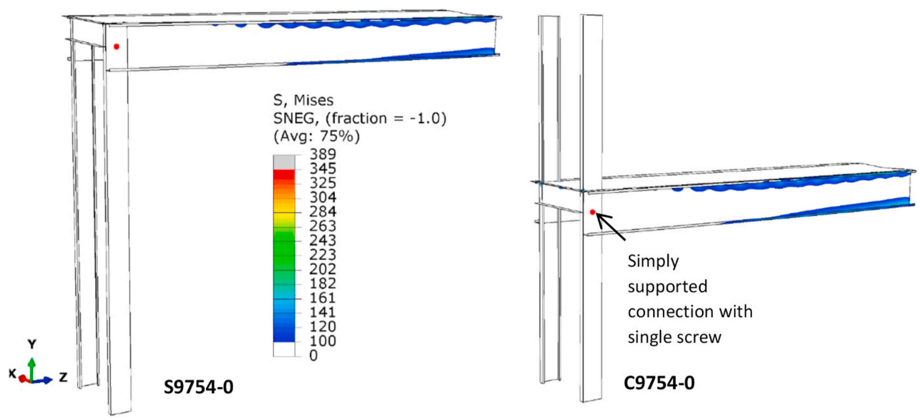

Fig. 11. Von-Mises stress contour greater than 100 MPa for S9754–0 and C9754-0 designs at $\alpha = 1$.

due to the deviations of the load-deformation behaviour of the fasteners in the tests and those incorporated in the FE taken from Refs. [7,11]. Furthermore, the contact behaviour between various steel-to-steel and OSB-to-steel surfaces in the ledger-framed connections might have deviated from that assumed in the FE simulations.

3.3. SFLS FE results and discussions

FE analysis was conducted for three sets of the joist and stud sections adopted from the joist-stud framed models in Section 2, corresponding to ranges of connection rotational stiffness within $k \leq 500$, $500 < k \leq 2000$ and $k > 2000$ kN m/rad (see Tables 1 and 2 for SCM and CCM, respectively). A semi-rigid SFLS connection has been designed using one to four vertical lines of screws for the identified ranges of connection rotational stiffness, each line having three #12 screws at the middle, top and bottom height of the connection (shown in Table 3). It should be noted that the choice of one to four vertical lines of screws is for consistency and comparison purposes and does not necessarily represent the optimum arrangements with the minimum number of screws. The FE models (listed in Table 3) are labelled with the start letter of S or C standing for the relevant construction method (SCM or CCM), followed by a 4-digit number representing the thicknesses of the joist and the stud sections of 1.4 mm (54), 1.8 mm (68) and 2.5 mm (97) ended by a single-digit number indicating the number of vertical lines of screws (1–4). In addition, two benchmark models of S9754–0 and C9754-0 were designed with one screw at the middle height of the SFLS connection corresponding to the $k = 0$ connection rotational stiffness in the joist-stud framed models in Section 2 adopted from CFS-NEES [2] with simply supported shear connection. The shear capacity of a single #12 screw connection is sufficient to transfer the design shear force based on DL + LL specified in Section 2.

3.3.1. Benchmark FE designs

Fig. 10 shows the DCRs for the benchmark models varying with the load ratio (α). The DCRs correspond to those limit states identified in the joist-stud framed designs (in Section 2) with the same labels of M, $M+V$ and D for the joists and $M+C$ for the studs. The load ratio, α, is the total applied floor and upper storey loads divided by the total design DL + LL loads with the same magnitudes as those utilised for the joist-stud framed designs in Section 2 which were adopted from CFS-NEES project [2]. As predicted in Section 2 for the frames with $k = 0$, the joist mid-span deflection limit state (shown by D in Fig. 10) dominates the design with DCR ratio close to unity at $\alpha = 1$. Shaded areas in Fig. 11 show the corresponding von-Mises stress distributions of the benchmark designs. For a better understanding of the most critical portions, the stress contour is set to display those areas greater than 100 MPa. As expected, the results are identical for both the S9754–0 and C9754-0 designs. By increasing the stress limit to 206 MPa (which is the level of stress calculated from the nominal yielding stress of 345 MPa divided by the design safety factor of 1.67), all the shaded areas are diminished. The results indicate an underutilised design strength of the joist and stud sections being dominated by the joist mid-span deflection and floor vibration for the simply supported joist-stud framed models, reflecting the CFS-NEES design [2].

3.3.2. Variation of connection rotational stiffness

Fig. 12 shows different levels of connection rotational stiffness varied with the load ratio of $\alpha = 0$ to 2, corresponding to various connection configurations having sets of one to four vertical screw lines (labelled by 1–4 shown by different line thicknesses). Also, the benchmark design using single screw connection (labelled by zero) is shown by dashed lines with connection rotational stiffness close to zero, mainly indicating the ignorable composite action between the joist and OSB. The connection rotational stiffness is derived by dividing the connection bending moment by the connection rotation; whereas, the connection

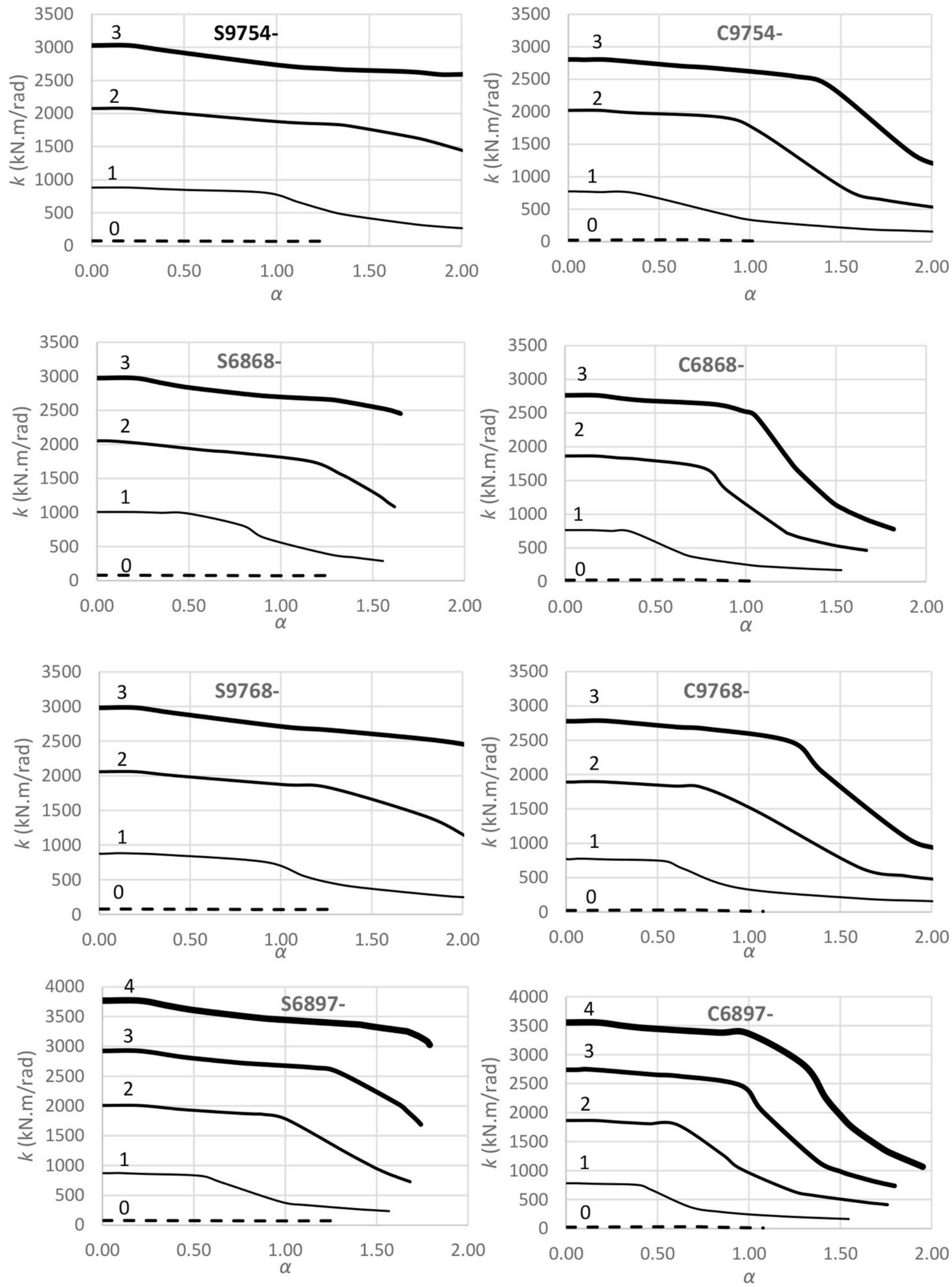

Fig. 12. Variation of the connection rotational stiffness, k, with the load ratio, α, for connections with one to four vertical lines of screws and the benchmark connection.

rotation is calculated by subtracting the stud contribution from the joist rotation at the connection centroid. As can be seen, the connection rotational stiffness slightly degrades by increasing the load ratio followed by a sharp degradation which is more noticeable in the CCM connections which also produce slightly lower initial connection rotational stiffness compared with that of the SCM connections. The initial degradation can be attributed to the local connection effects and diminishing of relatively small composite action between the joist and the flooring OSB due to the yielding of OSB-to-steel screws at the connection region. The afterwards sharp degradation occurs due to the yielding of the joist-to-stud connection screws, which is more critical for the connections with a lower number of screws for the CCM connections. A more detailed discussion is presented under section 3.3.5, where the screw forces of SCM and CCM connections are given.

Based on the connection rotational stiffness level at $\alpha = 1$, using one to four vertical lines of three #12 screws falls within the ranges of $k \leq 500$, $500 < k \leq 2000$ and $k > 2000$ kN m/rad specified in Tables 1 and 2 corresponding to the 97-54, 97-68, 68-68 and 68–97 joist-stud SCM and CCM designs. The FE results for each of the connection configurations are presented in the following subsections.

3.3.3. Overall designs

Tables 4 and 5 summarises the DCRs for all the SFLS connections within the whole range of the identified connection rotational stiffness at $\alpha = 1$, for SCM and CCM respectively. Three bands of DCRs have been specified indicating the design status and the material utilisation of the joists and studs. These are: DCR >1, $0.8 \leq$ DCR ≤ 1 and DCR <0.8, respectively refer to failed (denoted by F), efficient/economical design (denoted by E) and overdesigned (denoted by O) DCRs. Furthermore, the status of the screw shear forces in respect to the yielding force level

Table 4
DCRs for SFLS SCM connections.

Connection label	*k at α* = 1 (kN m/rad)	Joist			Stud	Screw shear forces
		M	*M* + *V*	D	*M* + *C*	
S9754-0	0	O	O	E	O	**U**
S9754-1	500–2000	O	O	O	**F**	**U**
S9754-2	500–2000	O	O	O	**F**	A
S9754-3	>2000	O	O	O	**F**	A
S6868-1	500–2000	**F**	E	**F**	**F**	**U**
S6868-2	500–2000	**F**	E	E	**F**	A
S6868-3	>2000	**F**	E	E	**F**	A
S9768-1	500–2000	O	O	O	E	**U**
S9768-2	500–2000	O	O	O	E	A
S9768-3	>2000	O	O	O	E	A
S6897-1	≤500	**F**	E	**F**	O	**U**
S6897-2	500–2000	**F**	E	E	E	A
S6897-3	>2000	**F**	E	E	E	A
S6897–4	**>2000**	**E**	**E**	**E**	**E**	**A**

Joist and stud design status: Failed (F), Efficient/economical (E) & Overdesigned (O).
Screw design status: Acceptable (A) & Undesirable (U).

Table 5
DCRs for SFLS CCM connections.

Connection label	*k at α* = 1 (kN m/rad)	Joist			Stud	Screw shear forces
		M	*M* + *V*	D	*M* + *C*	
C9754-0	0	O	O	E	O	**U**
C9754-1	≤500	O	O	O	E	**U**
C9754-2	500–2000	O	O	O	**F**	**U**
C9754-3	>2000	O	O	O	**F**	A
C6868-1	≤500	**F**	E	**F**	O	**U**
C6868-2	500–2000	E	E	E	E	**U**
C6868–3	**>2000**	**E**	**E**	**O**	**E**	**A**
C9768-1	≤500	O	O	O	O	**U**
C9768-2	500–2000	O	O	O	E	**U**
C9768-3	>2000	O	O	O	E	A
C6897-1	≤500	**F**	E	**F**	O	**U**
C6897-2	500–2000	E	E	E	O	**U**
C6897-3	>2000	E	E	O	O	A
C6897–4	**>2000**	**E**	**E**	**O**	**E**	**A**

Joist and stud design status: Failed (F), Efficient/economical (E) & Overdesigned (O).
Screw design status: Acceptable (A) & Undesirable (U).

at $\alpha = 1$, identified as one of the failure limit states, has been added being acceptable or undesirable (denoted by A or U). The successful designs, matching those presented in Section 2, are highlighted by grey colour, whilst the rest deemed unsuccessful designs due to the failed limit states or undesirable level of the screw shear forces. The results for successful designs as well as some examples of unsuccessful designs is discussed in more details in the following subsections.

3.3.4. Detailed designs for connections with one vertical line of three #12 screws

Fig. 13 shows the DCRs for the M, $M+V$, D and $M+C$ joist and stud limit states varied with the load ratio, α, for S9754–1 and C9754-1 models. At $\alpha = 1$ for S9754-1, the DCR for stud $M+C$ exceed the unity and may not be acceptable, while all the DCRs for C9754-1 are below one. These agree with the SCM, and CCM joist-stud framed designs with $k = 500$ kN m/rad in Tables 1 and 2, respectively. Another limit state that needs to be considered in the design is the shear failure of the screwed connections. Fig. 14 shows the screw shear forces (P_s) derived for the C9754-1 joist-to-stud fasteners normalised by the yielding load (P_{ny}) of 6.83 kN in Fig. 6. As can be seen, the top and bottom screws (shown by solid lines) reached the yielding force level at a loading ratio, α, less than unity. This is assumed herein as an undesirable limit state due to the residual deformation which could potentially occur under service loads over the lifetime of the structure. Therefore, the C9754-1 design with a single line of three #12 screws is also deemed unacceptable for the range of $k \le 500$ kN m/rad.

3.3.5. Detailed designs for connections with two to four vertical lines of three #12 screws

Fig. 15 shows the variation of DCRs with α for S9768-2& 3, C6868-2& 3, S6897–4 and C6897-4 designs chosen from Tables 4 and 5 with satisfactory joist and stud design limit states. As can be noticed, the SCM S9768-2& 3 designs are governed by the stud $M+C$ limit state with the DCR ratio close to unity, whilst the joists are designed conservatively. By increasing the vertical screw lines to 4, a more economic SCM design can be achieved with all the limit states being dominant in the S6897-4 design, thus more efficient design (highlighted in bold in Table 4). On the other hand, the CCM designs led to a more economic joist and stud DCRs reasonably close to unity for all the C6868-2, 3 and C6897-4 design cases. These results are consistent with those of the joist-stud framed designs presented in Section 2. As an example of failed/unacceptable designs for the ranges within $500 < k \le 2000$ and $k > 2000$ kN m/rad, Fig. 15 also shows the DCRs of the S6868-2& 3 models for which the joist M and the stud $M+C$ are both greater than unity at $\alpha = 1$. This design is consistent with the joist-stud framed design (in Section 2)

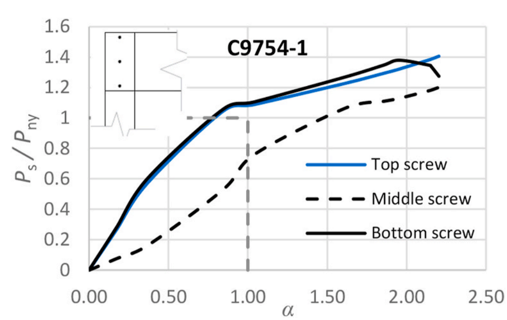

Fig. 14. Variation of screw shear forces with α for C9754-1 design.

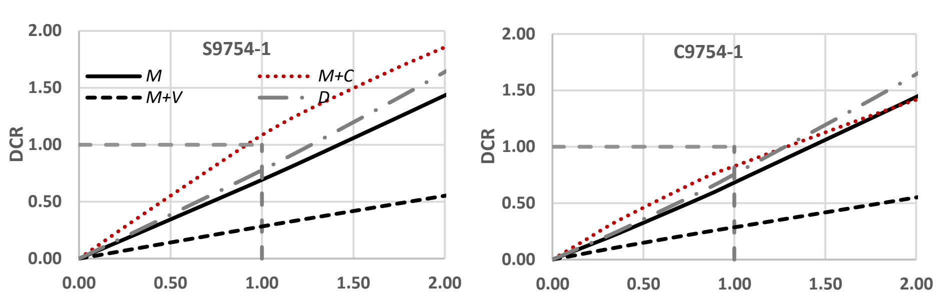

Fig. 13. Variation of DCRs with α for M, $M+V$, $M+C$ and D limit states for S9754–1 and C9754-1 designs.

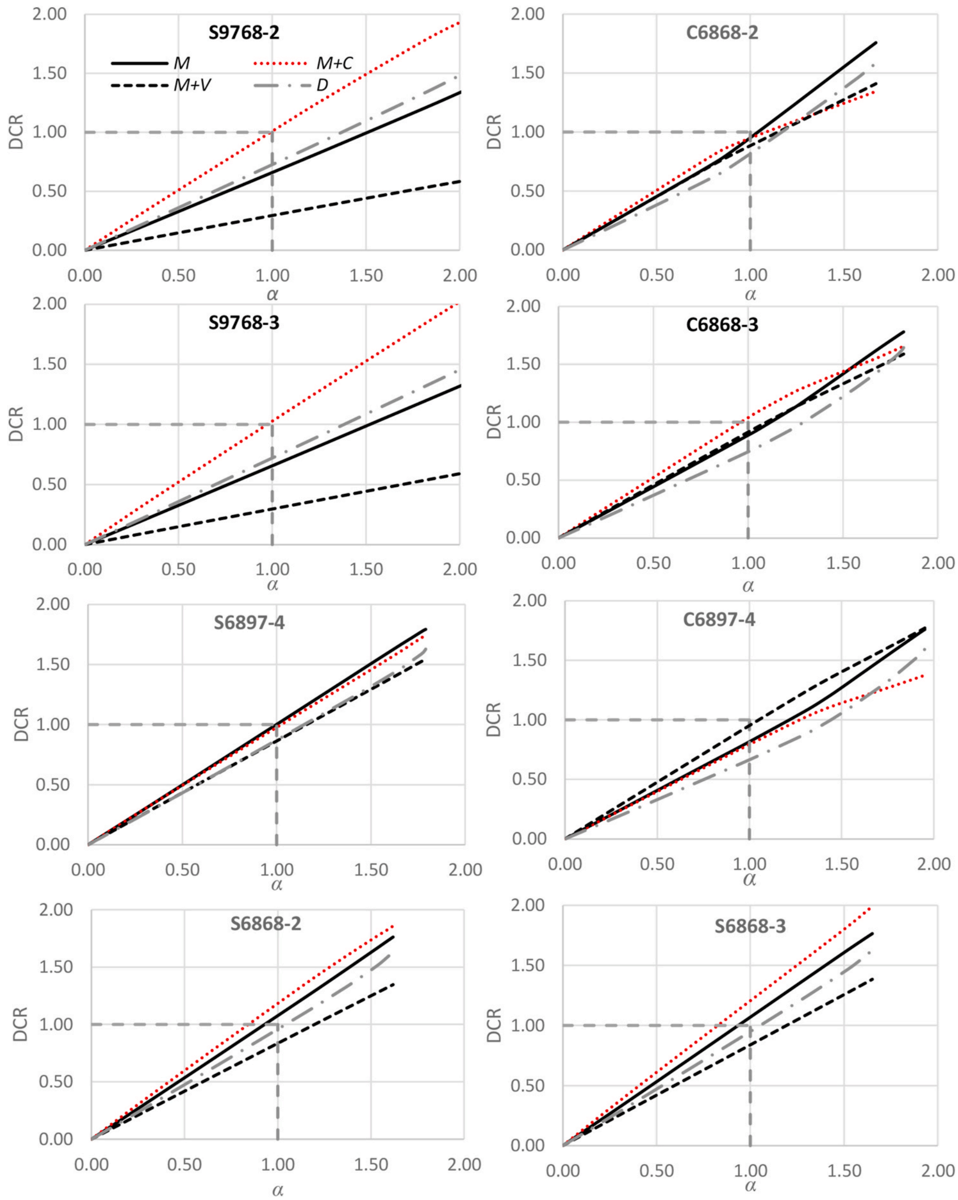

Fig. 15. Variation of DCRs with α for M, $M+V$, $M+C$ and D limit states for S9768-2& 3, C6868-2& 3, S6897–4, C6897–4, S6868–2 and S6868-3 designs.

which resulted in the heavier set of 97-68 joist and stud sections rather than the more economical 68-68 sections (like the CCM design).

Fig. 16 shows the normalised screw shear forces for the top, middle and bottom rows of screws of the S9768-2& 3, C6868-2& 3, S6897–4 and C6897-4 designs. These curves indicate an acceptable level of shear forces being lower than P_{ny} at $\alpha = 1$ for all the designs, except C6868-2 for which the shear forces of the top and bottom rows of screws reach P_{ny} at around $\alpha = 0.8$. The CCM designs, in general, led to higher screw shear forces than those of the corresponding SCM designs. This is due to the higher stud stiffness in the CCM designs, which led to lower stud rotation and as a result shifting the deformation demand to the connection. This means a higher CCM connection rotation at a certain load compared with that of the SCM connection. The higher deformation demand in the CCM connections than the SCM connections results in a generally slightly lower connection rotational stiffness and an earlier yielding in the CCM screws. This explains the more noticeable sharp degradation of the CCM connection rotational stiffness (observed in Fig. 12) as mentioned above. This may also lead to a higher number of screws for the CCM connections compared with that of the SCM connections to ensure elastic behaviour at $\alpha = 1$ as a desirable design requirement.

Fig. 16 also identifies the shear forces corresponding to each vertical lines of the screws for the CCM connections. As can be observed the last vertical line of screws from the connection end (denoted by the greatest vertical line number) attracts the greatest shear forces at each row of the screws. This is due to the superposition effect of the vertical components of the shear forces resulting from the connection shear and in-plane bending moment which are at the same and opposite directions for the last and first lines of the screws, respectively. Furthermore, the shear forces of the middle row of the screws pick up particularly after yielding of the top and bottom rows of screws which result in redistribution of the screw forces. It should be noted that the screw forces for the SCM connections follow a similar trend with more discrepancy between the top and bottom rows of screws which could be due to the more flexible nature of its supporting stud and consequential local effects compared with the CCM connections.

Fig. 17 shows the von-Mises stress distribution greater than 100 MPa (shown by shaded areas) for S6897–4 and C6897-4 designs at $\alpha = 1$. A larger spread of shaded areas achieved for both the S6897–4 and C6897-4 joist and stud designs compared with those of the simply supported

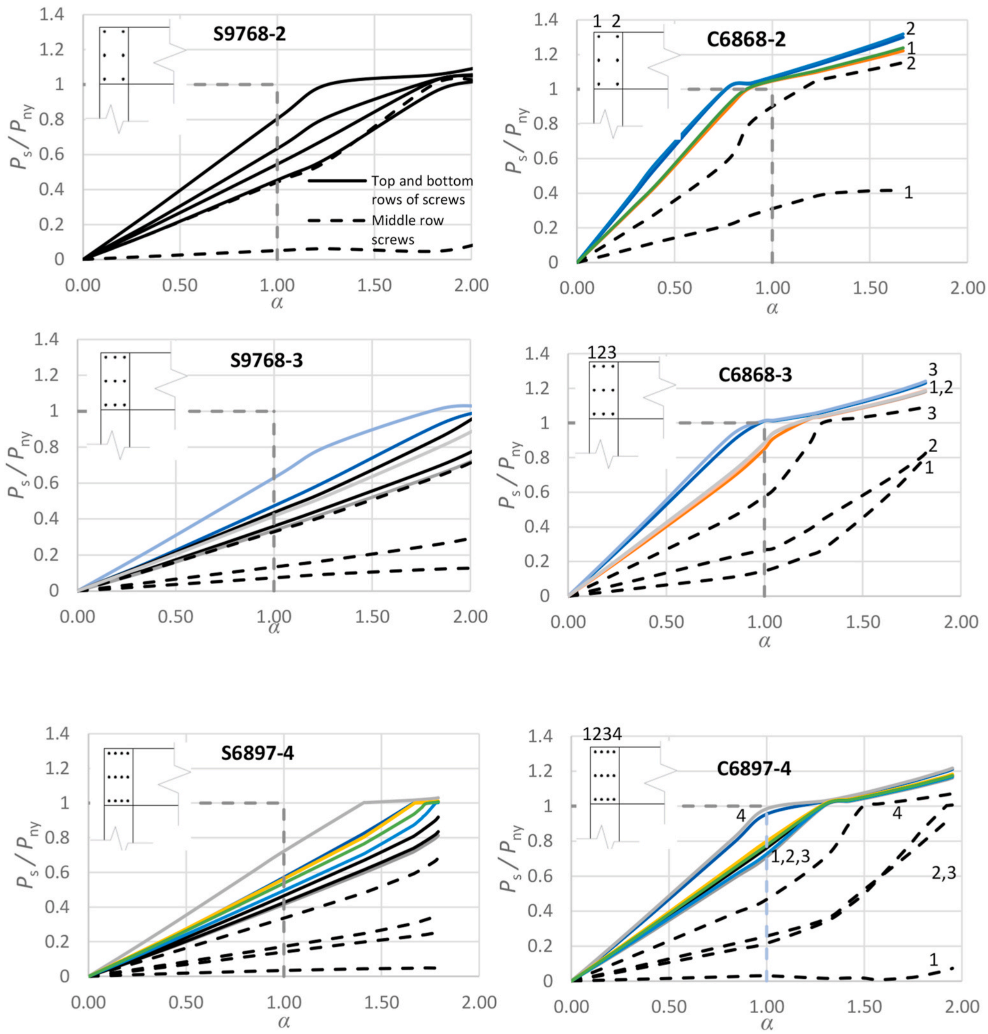

Fig. 16. Variation of screw shear forces with α for S9768-2& 3, C6868-2& 3, S6897–4 and C6897-4 designs (dashed lines: middle row screws, solid lines: top and bottom rows of screws).

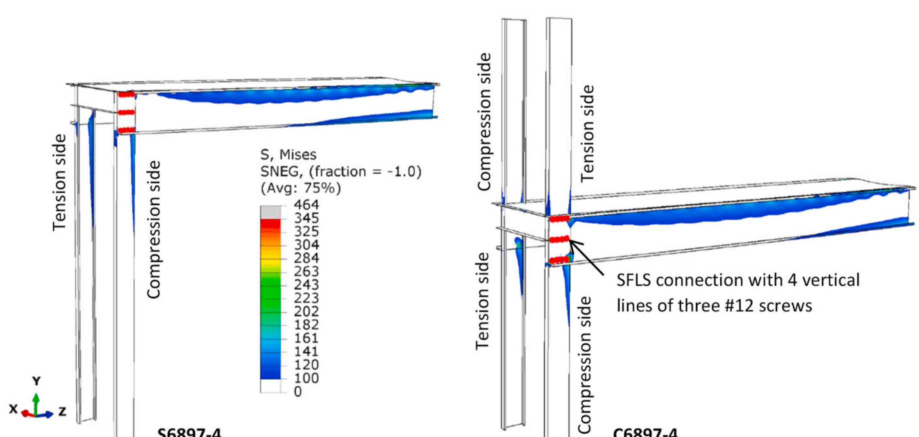

Fig. 17. Von-Mises stress contour greater than 100 MPa for S6897–4 and C6897-4 designs at $\alpha = 1.0$.

design counterparts (shown in Fig. 11, predominantly controlled by the joist mid-span deflection), thus a more efficient design (as reflected in Tables 4 and 5). As can be seen, the shaded areas are extended to the studs (mainly to the compression side of the lower storey) due to the bending moment transferred through the semi-rigid SFLS connections. This indicates the higher level of stud $M + C$ DCR compared with the overdesigned studs in simply supported connections. The simply supported designs could be even more inefficient for the conventional ledger-framed designs when accounting for the premature local failure effects (discussed in the introduction section).

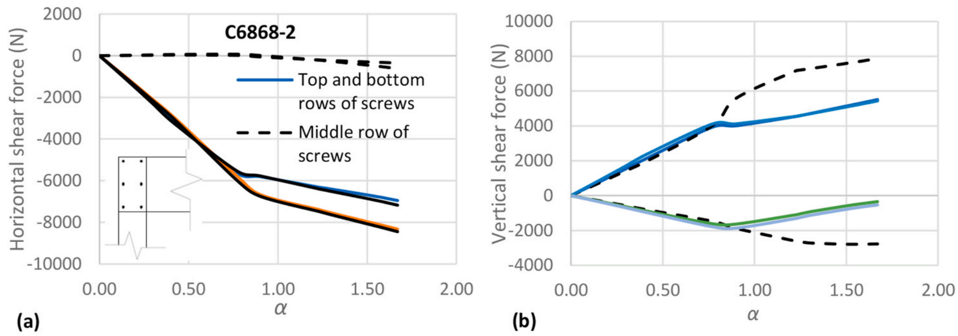

Fig. 18. Variation of horizontal and vertical screw shear forces with α for C6868-2.

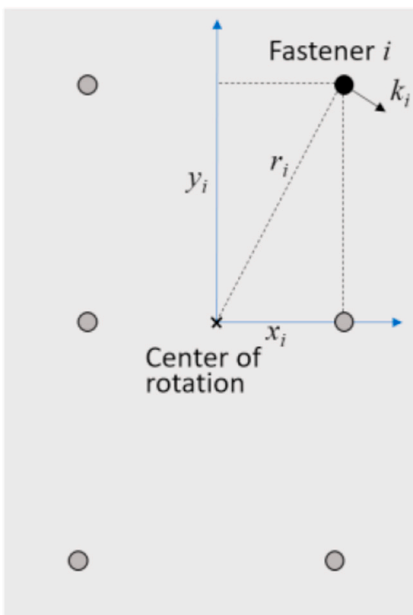

Fig. 19. Calculation of the connection rotational stiffness, k_c, for an arbitrary connection pattern.

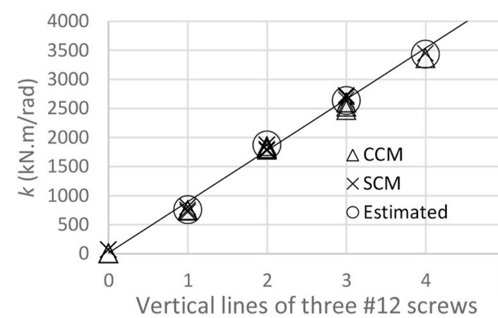

Fig. 20. Design connection rotational stiffness, k_c, for SCM and CCM connections with one to four lines of screws.

4. Connection rotational stiffness estimation

As it was shown in the previous sections, the magnitude of the connection rotational stiffness has a key role in the design of the developed semi-rigid connection for the developed SFLS system. To calculate the SFLS connection rotational stiffness a uniform force distribution is assumed within the joist-to-stud screw group. This can be an accurate assumption if the centre of rotation is located at the screw group centroid and the shear force is equally distributed between the screws. Fig. 18 (a) and 18(b) respectively show the horizontal and vertical screw force distribution of the representative C6868-2 model. As can be seen, the top and bottom rows of screws (shown by solid lines) attract almost the same horizontal force distribution (see Fig. 18 (a)), whilst the middle row horizontal forces (shown by dashed lines) are close to zero. These maintain up to around $\alpha = 0.8$ at which the top and bottom screws reach the yielding load (which can be cross-checked with the screw forces of C6868-2 model presented in Fig. 16). The vertical shear force distribution between the screws (shown in Fig. 18 (b)) also shows equal shear forces distributed between the left and right vertical lines of the screws, again up to $\alpha = 0.8$. Based on the horizontal and vertical screw force distribution, it can be concluded that the uniform force distribution assumption can be utilised for the estimation of the connection rotational stiffness before reaching the yielding load of the screws. As a design requirement, discussed in Section 3, the yielding load of the screws is desirable to be postponed after $\alpha = 1$ providing an elastic behaviour for the screws. This allows a more reliable design based on the simplified connection rotational stiffness estimation method for the SFLS connections.

For the design purposes, the connection rotational stiffness, k_c, is calculated based on a uniform screw group force distribution, using Eq. (1) and Fig. 19. This can be applicable for any arbitrary connection arrangement having n screws located at x_i and y_i distances from the screw group centre of rotation, while each screw has a shear stiffness of k_i in the force direction perpendicular to the radius of r_i for that screw.

$$k_c = \sum_{i=0}^{n} k_i r_i^2 = \sum_{i=0}^{n} k_i (x_i^2 + y_i^2) \tag{1}$$

Fig. 20 shows the connection rotational stiffness of both the CCM and SCM connections having one to four vertical lines of screws derived at $\alpha = 1$ or just before the yielding initiates in the screws. The estimated connection rotational stiffness, k_c, is shown by circles in Fig. 20. The connection rotational stiffness estimations well match a linear trendline for both the SCM and CCM connections.

5. Conclusions

Employing validated finite element (FE) analysis, a side-framed lightweight steel (SFLS) structure comprising semi-rigid floor-to-wall connections has been detailed and designed. Both the sequential and continuous construction methods (SCM and CCM) have been considered. A benchmark design having simply supported connections was chosen based on a recently tested ledger-framed floor-to-wall connections taken from the two-storey CFS-NEES project. Four design limit states were considered including the joist mid-span bending moment (M) and deflection (D), the joist end combined bending moment and shear force effect ($M + V$) and the stud combined bending moment and compression force effect ($M + C$). It was shown that the joist mid-span deflection (D) governed the benchmark design, which is consistent with the CFS-NEES design narrative, leading to underutilised strength of the joist sections. Incorporation of even a low level of connection rotational stiffness, adopted from the ledger-framed connection tests, into the design increases the stud demand-to-capacity ratio (DCR) by up to 22%. This means an unconservative design if the connection rotational stiffness is ignored.

Variation of the joist-to-stud connection rotational stiffness, k, from zero to fully fixed condition has led to three sets of joist-stud sections corresponding to three ranges of connection rotational stiffness. SFLS connection configurations with one to four vertical lines of three #12 screws matching the identified ranges of the connection rotational stiffness were then modelled and assessed. It was shown that, in general, CCM configurations could lead to more efficient designs than those of the SCM designs with both the joist and stud limit states being dominant. The stud $M + C$ limit state was predominant in the SCM designs within the lower range of connection rotational stiffness (corresponding to one to three vertical lines of three #12 screws). This, however, can be improved by using four lines of three #12 screws leading to an efficient design (like the CCM designs). On the other hand, a higher number of screws may be required for the CCM connections compared with the SCM connections to ensure an elastic connection design.

A simplified connection rotational stiffness estimation method has been examined based on the assumption of uniform screw force distribution. It was shown that the stiffness estimations agree well with those of the FE results for both the CCM and SCM designs.

Overall, the developed SFLS system comprising semi-rigid floor-to-wall connections is expected to provide a more efficient and economical design solution compared with the conventional LSF systems. The joist and stud material strengths are more significantly utilised through the semi-rigid connections with higher DCRs as opposed to the conventional designs governed by the joist mid-span deflection and premature local failures within the connection components. The joist-stud framed designs showed a 28% lighter flooring joist sections which together with the elimination of a ledger beam per side of the walls and clip angle connections per joist could lead to a more efficient LSF system. A trade-off is, however, required for optimising the joist and stud sections in the SFSL systems varying the joist-to-stud connection rotational stiffnesses.

More experimental studies can be very beneficial to validate the provided design method. Both the design methods provided in Ref. [3] and herein, are for when the stud is not interrupted by openings between the floors. In the case of having large openings, the effect of opening on the design of joist needs further studies.

Disclaimer

Any opinions, findings, and conclusions or recommendations expressed in this publication are those of the authors and do not necessarily reflect the views of the sponsors and employers.

Author statement

Alireza Bagheri Sabbagh: Conceptualization, Methodology, Software, Validation, Formal analysis, Investigation, Resources, Writing – original draft, Visualization, Shahabeddin Torabian: Conceptualization, Methodology, Validation, Investigation, Resources, Writing – review & editing, Visualization.

Declaration of competing interest

The authors declare that they have no known competing financial interests or personal relationships that could have appeared to influence the work reported in this paper.

References

[1] SCI Publication P402, Light Steel Framing in Residential Construction, 2015, 13: 978-1-85942-215-1.
[2] R.L. Madsen, N. Nakata, B.W. Schafer, CFS-NEES Building Structural Design Narrative, Research Report, 2011. RR01, access at, www.ce.jhu.edu/cfsnees.
[3] D. Ayhan, B.W. Schafer, Cold-formed steel ledger-framed construction floor-to-wall connection behaviour and strength, J. Constr. Steel Res. 156 (2019) 215–226.
[4] AISI, North American Standard for Cold-Formed Steel Structural Framing, American Iron and Steel Institute, Washington, Dc, 2015. AISI S240.
[5] Computers, I.N.C. Structures, SAP2000 Version 20.1.0, 2018. https://www.csiamerica.com/.
[6] Abaqus Analysis User's Manual, 2019 version 6.21.
[7] F. Tao, A. Chatterjee, C.D. Moen, Monotonic and cyclic response of single shear cold-formed steel-to-steel and sheathing-to-steel connections, 2016. Virginia Tech Report No. CE/VPI-ST-16-01.
[8] M. Shahini, A. Bagheri Sabbagh, P. Davidson, R. Mirghaderi, Development of cold-formed steel moment-resisting connections with bolting friction-slip mechanism for seismic applications, Thin-Walled Struct. 141 (2019) 217–231.
[9] A. Bagheri Sabbagh, M. Petkovski, K. Pilakoutas K, R. Mirghaderi, Development of cold-formed steel elements for earthquake resistant moment frame buildings, Thin-Walled Struct. 53 (2012) 99–108.
[10] A. Fieber, L. Gardner, L. Macorini, Structural steel design using second-order inelastic analysis with strain limits, J. Constr. Steel Res. 168 (2020) 1–19.
[11] H. Castaneda, K. Peterman, Moment-rotation response of cold-formed steel joist-to-ledger connections with variable finishes in ledger-framed construction, J. Constr. Steel Res. 176 (2021) 106396.